```
@inproceedings{orndorff2022investigation,
  author = {Nicholas C. Orndorff and John T. Hwang},
  title = {Investigation of Optimal Air-Taxi Transition Profiles using
    Direct-Transcription Trajectory Optimization},
  booktitle = {AIAA AVIATION 2022 Forum},
  year = {2022},
  doi = {10.2514/6.2022-3485},
  url = {https://doi.org/10.2514/6.2022-3485}
}
```

Investigation of optimal air-taxi transition profiles using direct-transcription trajectory optimization

Nicholas C. Orndorff* and John T. Hwang†
University of California San Diego, La Jolla, CA, 92093

The recent explosion of interest in a new vision of large-scale urban air travel has resulted in the introduction of hundreds of air-taxi concepts that are designed for vertical takeoff and landing. Many of these concepts combine wings and rotors to maximize performance in both cruising flight and hover. Smoothly transitioning between these two flight regimes is a dynamic process that must be accurately modeled to achieve high mission-level performance. The transition maneuver can be analyzed by formulating an optimal control problem. The most common solution approach, indirect transcription, is made difficult by the complexity of the model and the desire for constraints to be rapidly interchangeable in a practical design process. In this paper, we use direct transcription to convert the transition trajectory optimization problem to a nonlinear programming problem that we can solve using gradient-based optimization. The forward model incorporates nonlinear flight dynamics and blade element momentum rotor models. Using the resulting trajectory optimization algorithm, we perform numerical experiments on NASA's lift-plus-cruise air-taxi concept and its reference mission. First, to facilitate interpretation of our results, we propose a transition efficiency parameter, defined as the ratio of mechanical energy to total energy consumption. We also perform a refinement study involving the splines used to parametrize the control-variable profiles. This refinement study verifies that the error decreases monotonically, and the two finest parametrizations have an acceptable relative error of roughly 1%. We present optimized time-histories of several quantities of interest, which reveal that optimal trajectories are characterized by a full-power horizontal acceleration and a rapid decrease in power supplied to the lifting rotors. We also perform a sensitivity analysis of transition efficiency with respect to rotor disk loading, and find that a 10% increase in disk area translates to a roughly 1% increase in transition efficiency.

I. Nomenclature

u, w	=	body rates
θ	=	pitch angle
q	=	angular rate
x, z	=	Earth frame displacements
m	=	aircraft mass
g	=	gravitational acceleration
ρ	=	density
I_{yy}	=	aircraft moment of inertia
F_a, F_p	=	aerodynamic and propulsive forces
M_a, M_p	=	aerodynamic and propulsive moments
L, D	=	lift and drag
C_L, C_D	=	lift and drag coefficients
$C_{D,0}$	=	zero-lift drag coefficient
V	=	aircraft velocity
s	=	wing area
AR	=	aspect ratio
e_0	=	Oswald's efficiency factor
α	=	angle of attack
J	=	advance ratio
ϕ	=	inflow angle
σ	=	blade solidity
C_θ, C_x	=	radial and axial blade element coefficient
V_θ, V_x	=	rotational and axial free stream velocity
u_θ, u_x	=	rotational and axial induced velocities
B	=	number of rotor blades
c	=	rotor chord
r	=	rotor radial position
T	=	thrust
Q	=	torque
W	=	resultant inflow velocity
P	=	power
Ω	=	rotor rotational speed
$L_{1,2}$	=	lift rotor moment arms
η	=	transition efficiency
E	=	energy
n	=	number of time steps

*Graduate Student, Department of Mechanical and Aerospace Engineering, AIAA student member.
†Assistant Professor, Department of Mechanical and Aerospace Engineering, AIAA member.

II. Introduction

Trajectory optimization aims to find the control profiles that minimize a cost function while satisfying all given constraints. An optimal trajectory can be expressed as a set of control inputs ($\mathbf{u}^*(t)$) and states ($\mathbf{x}^*(t)$) that satisfies the constraints $c(t, \mathbf{x}, \mathbf{u}) = 0$. The system dynamics can be expressed as a function of the states and the input $\dot{\mathbf{x}} = f(t, \mathbf{x}, \mathbf{u})$. Within this system, an optimal trajectory minimizes the specified cost function $J(t, \mathbf{x}, \mathbf{u})$.

Solving a trajectory optimization problem to predict the transition maneuver of an electric vertical-takeoff-and-landing aircraft (eVTOL) is difficult due to the nonlinear nature of the flight dynamics during transition. A number of prior studies in the literature investigate alternate options other than trajectory optimization for solving the optimal control problem. Ritz and D'Andrea [1], Jung and Shim [2], and Hartmann et al. [3] all proposed (and demonstrated) global controllers based on robust linear controllers and look-up tables for gain scheduling. Cook and Hauser [4] proposed a similar method based on a time-varying linear quadratic regulator. Unified controller strategies comprised of single nonlinear controllers have been proposed by Raab et al. [5] and Zhou et al. [6]. Zhou et al. [6] proved global asymptotic stability of the controller, implying robustness. Casau et al. [7] further explored nonlinear controllers by proposing three different nonlinear controllers for the three distinct flight regimes for eVTOL aircraft (hover, transition, and cruise). In addition, they proved their controllers were input-to-state stable.

Trajectory optimization problems can be solved using indirect or direct transcription. Indirect transcription is the differentiate-then-discretize approach, where optimality conditions are hand-derived in an ad hoc fashion given the specifics of the optimization problem. This approach is advantageous because of its speed, but a key drawback is that the optimality conditions need to be re-derived whenever the objective function, constraints, or design variables are changed, for instance, in a practical design cycle. On the other hand, direct transcription is the discretize-then-differentiate approach, where discretization leads to a nonlinear programming (NLP) problem that can be solved by a general-purpose, off-the-shelf optimizer [8]. Recent advances have automated the process of deriving and implementing derivatives needed for gradient-based optimization. Therefore, direct transcription is well-suited to use in a practical design setting, in which the optimization problem needs to be frequently modified.

The direct transcription method represents the control input as a piecewise function of time, thereby allowing the optimizer to act as the controller. The resultant trajectory is then evaluated with respect to the constraints and objective function. The direct transcription approach has been demonstrated for eVTOL transition trajectory optimization by Chauhan and Martins [9] and Anderson et al. [10]. Yang et al. [11] combined an NLP trajectory optimization problem with a robust linear controller, proving that an optimal reference trajectory can be reliably tracked in simulations. Piprek and Holzapfel [12] paired a gradient-based optimizer with a genetic algorithm in an effort to find a globally optimal trajectory for a small drone.

One common objective function for transition trajectory optimization is the transition time. Minimum-time transition trajectories were explored by Stone and Clarke [13], who found that optimal trajectories were strongly influenced by aircraft mass. Stone et al. [14] verified their findings with flight tests. Banazadeh et al. [15] evaluated minimum-time transition trajectories for a thrust-vectored tail-sitter aircraft, discovered the aircraft was unstable and proposed a robust optimal control scheme. Additional work by Banazadeh and Taymourtash [16] used NLP and gradient-based optimization to evaluate the same aircraft. Kubo and Suzuki [17] found that control surfaces and high lift devices were critical to minimizing transition time without a significant decrease in altitude. They also showed that high throttle settings prevented the stalling of the wing during the high-angle-of-attack maneuvers seen during transition. Zhong and Wang [18] who also examined minimum-time transitions for a tail-sitter UAV found that increases in mass or the drag coefficient increased the transition time and altitude variation. Li et al. [19] evaluated the differences between an un-optimized linear transition and a minimum-time transition trajectory for a small tail-sitter UAV. Through simulations and experimental results, they found that the optimized trajectories were superior.

Another common objective function for transition trajectory optimization is energy. Chauhan and Martins [9] evaluated minimum energy transition trajectories for the Airbus Vahana eVTOL concept. They investigated the effect of various stall and acceleration constraints, and determined that (a) the effect of stall constraints was negligible, (b) acceleration constraints significantly reduced the amount of power supplied to the motors, and (c) unconstrained transition trajectories were characterized by full-power accelerations. Anderson et al. [10] found minimum energy transition trajectories and studied the effect of model fidelity on the optimization results.

Constant altitude transition maneuvers were included by Silva et al. [20] as part of a typical mission profile developed for NASA's eVTOL common research models. Maqsood and Go [21] evaluated optimal constant-altitude transition trajectories, and found that elevator effectiveness plays an important role in minimizing altitude variation. Oosedo et al. [22] minimized constant-altitude transition time for a tail-sitter UAV, explored various control strategies, and verified their results with scaled flight tests. Verling et al. [23] and Pradeep and Wei [24] investigated constant-altitude reverse transitions (i.e., cruise to hover). Both noted that optimal trajectories involve significant altitude variation.

Typical aerodynamic and rotor models for trajectory optimization problems are low-fidelity because of the need to reduce computation time. Anderson et al. [10] compared the effects of model fidelity on a trajectory optimization problem. They compared two approaches to model rotor-wing interactions: (1) a low-fidelity momentum-based model and (2) a mid-fidelity blade-element-momentum (BEM) and vortex lattice method (VLM). They found that the mid fidelity BEM-VLM model more conservatively and accurately predicted stall performance. They concluded by noting that the BEM-VLM model was too complex to implement within their transition trajectory optimization model.

Whereas most current research on trajectory optimization has focused on small UAVs, research on trajectory optimization for larger eVTOL concepts has been limited. Notably, Rothhar et al. [25] worked to model and optimize trajectories for the NASA GL-10 prototype, Chauhan and Martins [9] evaluated the Airbus Vahana concept, and Hwang and Ning [26] modeled NASA's X-57 Maxwell demonstrator.

In this paper, we find minimum-energy constant-altitude transition trajectories for the NASA lift-plus-cruise eVTOL concept. We use direct transcription to describe the optimal control problem as an NLP problem, enabling the use of a commercial gradient-based optimizer to find the optimal trajectories. The lift-plus-cruise aircraft is modeled with low-fidelity aerodynamic approximations, and the rotors are modeled with a BEM method developed by Ruh and Hwang [27]. This BEM method is robust and has been proven in an optimization environment. Flight dynamics are modeled with a three-degree-of-freedom nonlinear system of ordinary differential equations (ODEs). These ODEs are solved and differentiated using the general linear methods (GLM) formulation following Hwang and Munster [28] and the modular analysis and unified derivatives (MAUD) approach developed by Hwang and Martins [29].

We begin this paper by discussing the methods used to model NASA's lift-plus-cruise aircraft. We then formulate the optimization problem by describing the objective function, design variables, and constraints. Next we present the results which include time histories of the design variables and aircraft states and are accompanied by a brief discussion. After finding a nominal minimum-energy transition trajectory, we end by exploring the effect of varying rotor disk loading on transition efficiency.

III. Methodology

A. Flight Dynamics

We model aircraft dynamics with a three-degree-of-freedom nonlinear flight simulation. The governing equations consist of six first-order ordinary differential equations (Eqs. 1-6) [30]. All external forces and moments are separated into their aerodynamic and propulsive components $(F_a + F_p)$ and $(M_a + M_p)$. The linear body rates are u and w, the pitch angle, θ, the angular velocity, q, and the Earth-frame displacements, x and z. The state equations are given by

$$\dot{u} = -qw - g\sin(\theta) + (F_{ax} + F_{px})/m \tag{1}$$

$$\dot{w} = qu + g\cos(\theta) + (F_{az} + F_{pz})/m \tag{2}$$

$$\dot{\theta} = q \tag{3}$$

$$\dot{q} = (M_a + M_p)/I_{yy} \tag{4}$$

$$\dot{x} = u\cos(\theta) + w\sin(\theta) \tag{5}$$

$$\dot{z} = u\sin(\theta) - w\cos(\theta), \tag{6}$$

and the full state vector is given by

$$\mathbf{x} = [u\ w\ \theta\ q\ x\ z]^T. \tag{7}$$

These six equations are solved using the ODE solver Ozone, which uses the general linear methods formulation [28]. Among the large list of available methods, we choose the explicit-midpoint method for the results presented in this paper.

Since model-level derivatives are needed for gradient-based optimization, an important consideration for this approach is to ensure derivatives can be provided in each part of the model. In this case, partial derivatives of the six state equations are implemented along with the ODEs' right-hand sides. Ozone combines these derivatives and propagates them through the time-marching process backward-in-time. Next, Ozone's derivatives are assembled, along with the partial derivatives of pre- and post-processing computations before and after the ODE solution occurs in the model. This assembly and, ultimately, the computation of total derivatives of the model are performed using the MAUD approach [29].

B. Wing Aerodynamics

This study considers NASA's lift-plus-cruise air-taxi concept [20] (Fig. 1). This aircraft has eight lifting rotors, a single cruise rotor, a high-wing, and standard empennage. The pylon-mounted lift rotors are situated such that wing-rotor interactions are minimal.

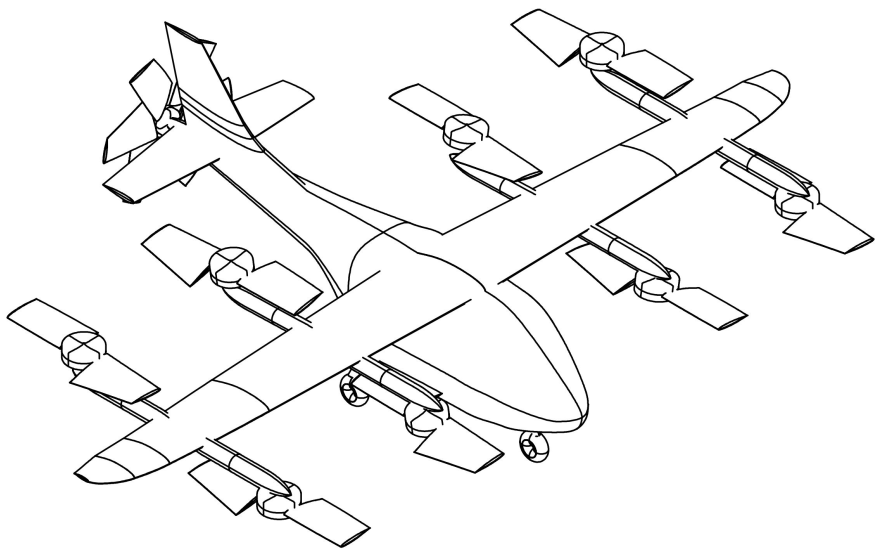

Fig. 1 NASA's lift-plus-cruise air-taxi concept [20].

Lift L and drag D are calculated from standard formulas. Density ρ is calculated with the standard atmospheric model. The wing area is denoted by S, the aspect ratio, by AR, the zero-lift drag coefficient, by C_{D_0} and Oswald's efficiency factor, by e_0. Lift and drag are given by

$$L = \frac{1}{2}\rho V^2 S C_L \tag{8}$$

$$D = \frac{1}{2}\rho V^2 S C_D \tag{9}$$

$$C_D = C_{D_0} + \frac{{C_L}^2}{\pi A R e_0}. \tag{10}$$

These aerodynamic forces act in the wind axis system and must be transformed into the body axis system before they can be input to the flight dynamics model. We transform these forces by calculating the angle of attack α and then compute the two components of the aerodynamic forces F_{ax} and F_{az} in the body axes:

$$\alpha = \arctan(w/u) \tag{11}$$

$$F_{ax} = -D\cos(\alpha) + L\sin(\alpha) \tag{12}$$

$$F_{az} = -D\sin(\alpha) - L\cos(\alpha). \tag{13}$$

For this simplified model, aerodynamic moments are not considered, and the empennage and its associated forces are ignored. Aircraft properties are shown in Table 1. These properties consist of data from NASA [20] as well as estimated parameters.

Table 1 Aircraft properties

Mass	3724 kg
Lift rotor radius	3.2 m
Cruise rotor radius	2.85 m
C_{D0}	0.0151
Wing area	39 m^2
Aspect ratio	11.2
Oswald's efficiency factor	0.8
Wing lift slope	$2\pi\ rad^{-1}$

C. Rotor Aerodynamics

We model the lift and cruise rotors with the BEM implementation developed by Ruh and Hwang [27]. Each rotor blade is discretized radially, and the inflow angle is solved at each discretization point using a bracketed search algorithm that is guaranteed to converge, which is applied to the following residual function:

$$R(\phi) = \frac{J}{\pi}(\sigma C_\theta + 4\sin(\phi)\cos(\phi)) + (\sigma C_x - 4\sin^2(\phi)). \tag{14}$$

Once the inflow angle distribution is known, then the induced radial and axial velocities (u_θ and u_x) can be calculated as follows:

$$u_\theta = \frac{2\sigma C_\theta V_\theta}{4\sin(\phi)\cos(\phi) + \sigma C_\theta} \tag{15}$$

$$u_x = V_x + \frac{\sigma C_x V_\theta}{4\sin(\phi)\cos(\phi) + \sigma C_\theta}. \tag{16}$$

The local blade solidity σ, and the rotational rotor velocity V_θ are calculated with the following equations:

$$\sigma = \frac{Bc}{2\pi r} \tag{17}$$

$$V_\theta = \Omega R. \tag{18}$$

Thrust and torque are calculated using any one of the primary BEM equations in Table 2 summed over the rotor radial discretization. Rotor power can be calculated from the torque Q and the rotor rotational speed Ω via the equation $P = Q\Omega$. The airfoil model used within the blade element calculations is extracted from a pre-compiled data set and parameterized with a spline-based surrogate model [31] to create a smooth piecewise function for the rotor lift and drag coefficients.

Table 2 Summary of BEM equations [27]

Theory	Thrust	Torque
Axial Momentum	$dT = 4\pi\rho u_x(u_x - V_x)rdr$	NA
Angular Momentum	$dT = 2\pi\rho(V_\theta - 0.5u_\theta)u_\theta rdr$	$dQ = 2\pi\rho u_x u_\theta r^2 dr$
Blade Element	$dT = 0.5C_x\rho W^2 Bcdr$	$dQ = 0.5C_\theta\rho W^2 Bcrdr$

The lift and cruise rotors align with the aircraft body axes and the resultant propulsive forces and moments can be passed directly into the flight dynamics model. To minimize the computational complexity of the BEM model we only analyze one rotor from each lifting group as shown in Fig. 2. The lift rotors are placed in two groups of four rotors each. The cruise rotor thrust is T_{cruise}, the lift rotor thrust is T_{lift}, and the moment arms are L_1 and L_2 respectively. The following equations sum the forces and moments due to the rotors:

$$F_{px} = T_{cruise} \tag{19}$$

$$F_{pz} = 4T_{lift,1} + 4T_{lift,2} \tag{20}$$

$$M_p = 4T_{lift,1}L_1 - 4T_{lift,2}L_2. \tag{21}$$

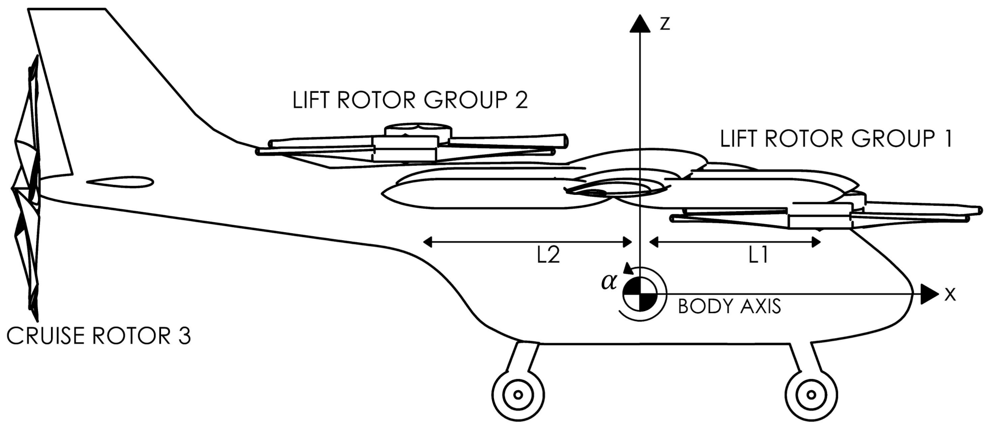

Fig. 2 Rotor groups for the lift-plus-cruise aircraft.

D. Optimization Problem and Direct Transcription

In this paper, we find the minimum-energy constant-altitude transition trajectories for the NASA lift-plus-cruise eVTOL concept. If we represent the system dynamics by $\dot{\mathbf{x}}(t) = f(t, \mathbf{x}(t), \mathbf{u}(t))$, then the solution to the optimal control problem minimizes the following cost function:

$$\begin{aligned} \underset{\mathbf{u}(t)}{\text{minimize}} \quad & E = \int_{t_i}^{t_f} \left(P_1(t, \mathbf{x}(t), \mathbf{u}(t)) + P_2(t, \mathbf{x}(t), \mathbf{u}(t)) + P_3(t, \mathbf{x}(t), \mathbf{u}(t))\right) \, dt \\ \text{subject to} \quad & c_p(t, \mathbf{x}(t), \mathbf{u}(t)) \leq 0 \\ & c_t(t_f, \mathbf{x}(t), \mathbf{u}(t)) = 0 \end{aligned} \tag{22}$$

where E represents energy and P_1, P_2, P_3 represent the rotor power for the two lift rotor groups and single cruise rotor. The trajectory is subject to path and terminal constraints denoted by c_p and c_t respectively.

We use direct transcription to convert this problem to an NLP problem in discrete time. The discrete time-step is Δt and the number of time-steps is n. The following optimization problem can be solved with gradient-based optimization:

$$\begin{array}{rll} \underset{\vec{u}, \Delta t}{\text{minimize}} & E(\vec{t}, \vec{x}, \vec{u}) & \text{(objective function)} \\ \text{subject to} & c_p(\vec{t}, \vec{x}, \vec{u}) \leq 0 & \text{(path constraints)} \\ & c_t(\vec{t}, \vec{x}, \vec{u}) = 0 & \text{(terminal constraints)} \\ \text{with} & \vec{t} = [t_i, t_i + \Delta t, t_i + 2\Delta t, \ldots, t_i + n\Delta t] & \text{(discrete times vector)} \end{array} . \tag{23}$$

The input to the BEM rotor model is rotor rotational speed, which is parametrized with cubic splines. The control points for these splines are the design variables in the optimization problem. There are three splines in total, one for the cruise rotor and two for the lifting rotor groups. Natural cubic splines were chosen because of the simplicity of implementation. We solve for the spline coefficients with a system of linear equations and then interpolate the spline using the time step Δt and the number of time steps n. The Ozone ODE solver becomes increasingly robust with a decreasing Δt, leading to a choice of $n = 30$, a number that was empirically determined such that the optimizer could reliably reach convergence. The time step Δt is included as a design variable of the optimization problem since different trajectories may satisfy the terminal constraints at different times. Table 3 presents the objective, design variables, and constraints in more detail. Numeric constraints on power and velocity are taken from data presented by Silva et al. [20].

Table 3 Optimization problem formulation

	Function/variable	Notes	Quantity
Objective	Energy		1
Design Variables	Lift rotor speed	Cubic splines (2 splines, 8 control points)	16
	Cruise rotor speed	Cubic spline (1 spline, 8 control points)	8
	Transition time	Integrator Δt	1
Constraints	Lift power	$0 < P_{lift} < 103,652W$	2
	Cruise power	$0 < P_{cruise} < 468,300W$	2
	Final altitude	$z_f = z_i$	1
	Final horizontal velocity	$\dot{x}_f > 45ms^-1$	1
	Final angular velocity	$q_f = 0$	1
	Final lift power	$P_{lift,f} = 0$	1
	Pitch angle	$-0.1 < \theta < 0.1rad$	2

The aircraft starts from a near-hover condition. The initial horizontal body velocity u_0 is set to 0.1 m/s in order to avoid a zero denominator when calculating angle of attack. The initial pitch angle θ_0 and angular rate q_0 are zero. Final lift rotor power is set to zero, to ensure the aircraft relies on aerodynamic lift at cruise velocity.

Energy is added as an extra state within the system of ordinary differential equations in Ozone. The objective of this optimization problem is to minimize total energy, which is is defined as the final entry in the resulting state vector. Eq. (24) presents the state equation for energy as a function of lift and cruise power:

$$\dot{E} = P_{lift} + P_{cruise}. \tag{24}$$

We solve this optimization problem with gradient-based optimization and adjoint-based derivative computation. The adjoint method scales well with the number of design variables and is well suited for this problem. The optimizer used is SNOPT-7.7 [32], with major optimality and major feasibility set to $1E - 1$. This optimization problem is computationally intensive, primarily due to the inclusion of the BEM rotor model. A typical optimization takes 2-10 hours to converge on a laptop computer.

E. Transition Efficiency

To facilitate comparisons between different trajectories, we define a new transition efficiency parameter η in Eq. (25) as the ratio of the increase in mechanical energy (kinetic plus potential energy) to the total energy consumed by the aircraft:

$$\eta = \frac{0.5m\Delta V^2 + mg\Delta h}{E_{total}}. \tag{25}$$

With this parameter we can compare optimal trajectories for a variety of aircraft and aircraft configurations.

In this paper the final velocity is defined by a terminal constraint. Since our transition is constant-altitude, the change in potential energy is zero. Therefore, the principal impact of an optimal transition is in the denominator of Eq. (25). Eq. (25) is non-dimensional, and is valid for any aircraft trajectory with a different initial and final velocity and/or altitude. Note that Eq. (25) is equivalent to the ratio of the specific energies, that is, the ratio of the sum of the specific changes in kinetic and potential energies per unit mass, in the numerator, to the specific total energy consumed per unit mass, in the denominator.

IV. Results

A. Nominal Case

An optimal constant-altitude minimum-energy transition trajectory is presented here for the lift-plus-cruise aircraft. The aircraft starts from hover at a 100 m altitude and near-zero velocity and reaches a cruising velocity of 46 m/s, 13.49 seconds later. Using the efficiency parameter defined in Eq. (25), we find a transition efficiency of 24.67%. Table 4 presents the transition efficiency, total energy consumed, and the transition time for this trajectory.

Table 4 Summary of optimization results

Transition efficiency η	24.67 %
Total energy E	16.18 MJ
Transition time	13.49 s

The design variables of the transition optimization problem consist of three splines parametrizing the rotor speed profiles. These splines and the corresponding rotor power are plotted in Fig. 3 along with the maximum available cruise power. We note that cruise power is maximized at 468,300 W for the first half of the transition while the combined lift power is significantly lower than the 8×103,652 W limit (eight rotors at 103,652 W maximum per rotor). Lift rotor speed is non-zero for the duration of the transition despite the fact that lift power decreases to zero halfway through the transition maneuver. Rotor power is calculated from the BEM model and is a function of the rotor speed as well as the aircraft velocity. Any differences between the rotor speed plots and the rotor power plots likely stems from the effect of velocity on the power calculation.

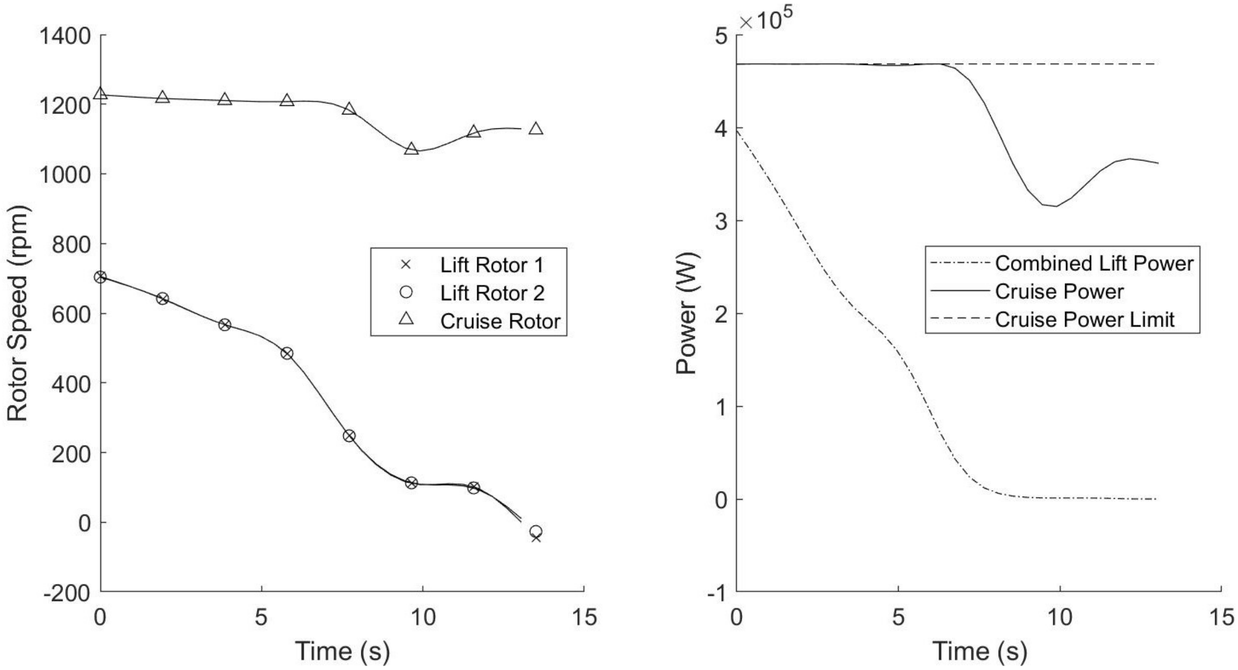

Fig. 3 Optimal rotor speed profiles and corresponding rotor power.

The six states of the flight dynamics model (u, w, θ, q, x, z) are plotted in Fig. 4 along with angle of attack α and the lift force L for the optimal transition trajectory. We find that the aircraft initially pitches up until the maximum pitch constraint is reached at 5.7°. The aircraft remains in this nose-up attitude until the end of the transition when the aircraft pitch decreases. We hypothesize that the aircraft pitches up to maximize the angle of attack so as to produce more lift at lower velocities. Towards the end of the transition the design angle of wing incidence provides sufficient lift without an increase in pitch angle. The angular rate q is defined in Eq. (3) as the time-derivative of the pitch angle. We see from Fig. 4 that q reaches a maximum of three degrees per second as the aircraft pitches up at the start of the transition. The return to a lower pitch angle at the end of the transition is performed at two degrees per second. The final angular rate q_f is constrained to be zero as presented in Table 3 and verified in Fig. 4.

Vertical body velocity w is near-zero for the duration of the transition. Slight fluctuations in w are due to changes in pitch angle, causing the body velocity vectors to rotate with respect to the fixed Earth axes and to couple with other velocity components. Horizontal body velocity u increases steadily to a cruise speed of 46 m/s. For this optimization there are no constraints on final horizontal or vertical acceleration. This explains why the horizontal velocity does not level off asymptotically towards the end of the transition maneuver.

The altitude z stays constant throughout the transition. This is expected for a minimum-energy trajectory but not guaranteed since there are no path constraints on altitude. Horizontal displacement x grows monotonically reaching 356 m by the end of the transition. Horizontal displacement is unconstrained, and is a function of the body velocity and pitch angle as defined in Eq. (5).

Angle of attack α and the lift force L are functions of the six system states and therefore mirror some of the trends that appear elsewhere. Angle of attack increases for the duration of the transition roughly copying the pitch angle θ. Lift force increases steadily and begins to fluctuate once velocity increases sufficiently for the wing to support the aircraft without the aid of the lifting rotors. This fluctuation is also visible in the cruise rotor speed spline towards the end of the transition. During this fluctuation the lift force overshoots the aircraft weight by 3.7‰ and the horizontal velocity overshoots the terminal velocity constraint by 1 m/s. We hypothesize that this overshoot could be resolved by reducing the optimizer convergence tolerance.

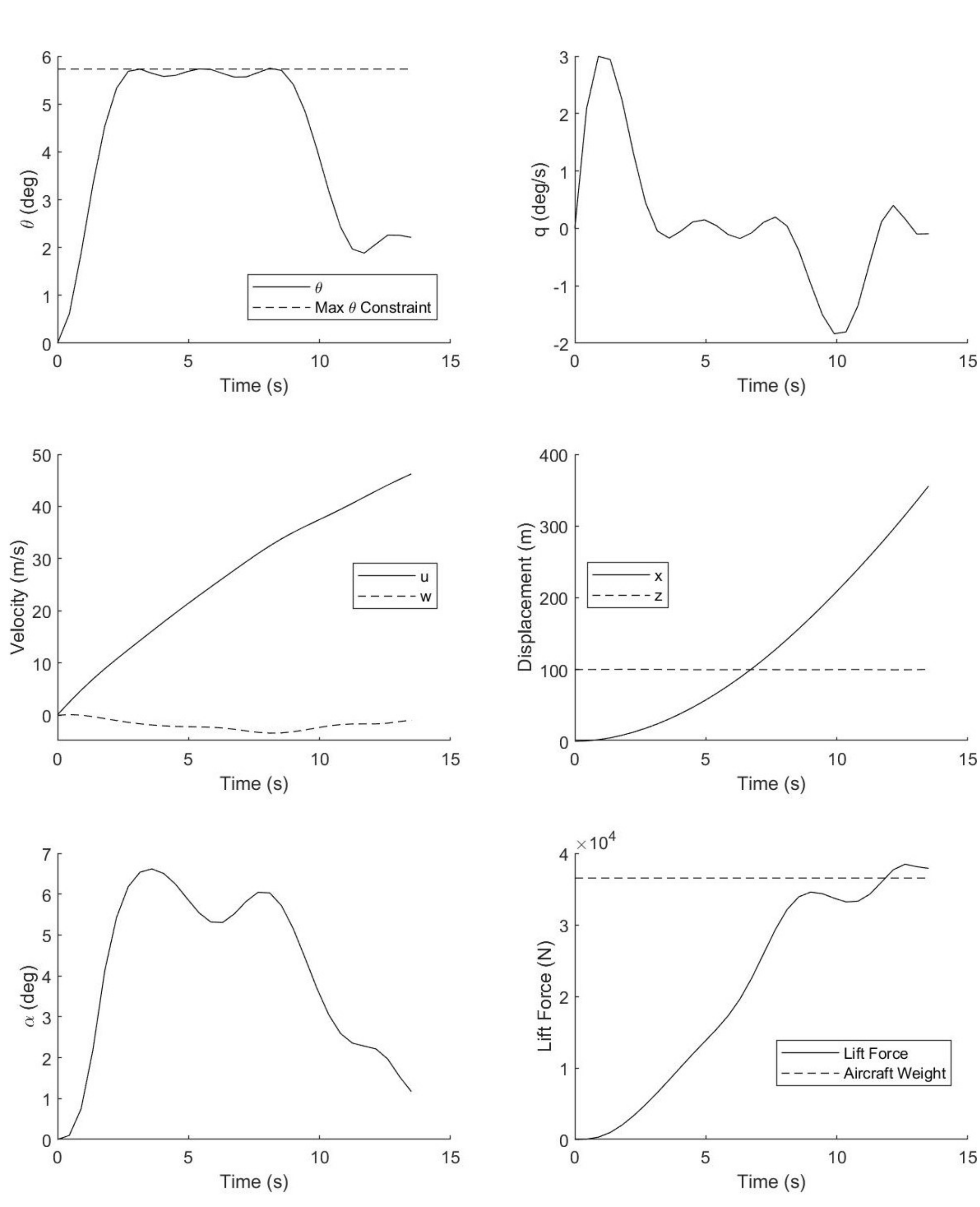

Fig. 4 Time-histories for the optimal minimum-energy transition trajectory.

B. Verification of the Spline Parametrization

Here we perform a spline refinement study to evaluate the effect of increasing numbers of spline control points on the optimal transition trajectory. This study is intended to verify the results of the transition optimization and provide guidance on the appropriate number of control points to use in further work. The transition optimization problem is consecutively solved for the lift-plus-cruise aircraft with rotor speed parametrized by splines with between 4 and 24 control points. The optimal results for the 24 control point spline are taken as a datum and the relative error between the datum and every other optimal spline is plotted on the logarithmic graph in Fig. 5. We can see that the relative error decreases monotonically, and the two finest parametrizations (with 20 and 22 control points) have a relative error of roughly 1%. This lends confidence to the methods and models used in this paper.

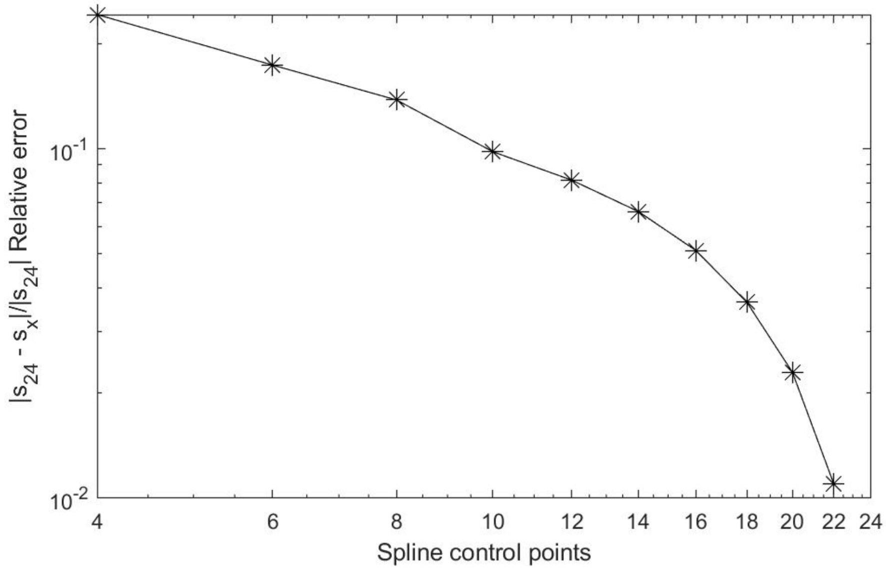

Fig. 5 Relative error between optimal splines with increasing control points.

C. Sensitivity Study

To evaluate the effect of rotor disk loading on transition efficiency we compare minimum-energy transition trajectories for the lift-plus-cruise aircraft modified with a range of cruise and lift rotor diameters. We vary the cruise rotor diameter between 2.625 m and 4.25 m and all eight lift rotor diameters are identically varied between 2.625 m and 4.5 m in 0.125 m increments. The corresponding disk loading is calculated as $mg/(\pi r^2)$ where the aircraft mass is constant. We calculate transition efficiency from Eq. (25) and plot the results of this sensitivity study in Fig. 6.

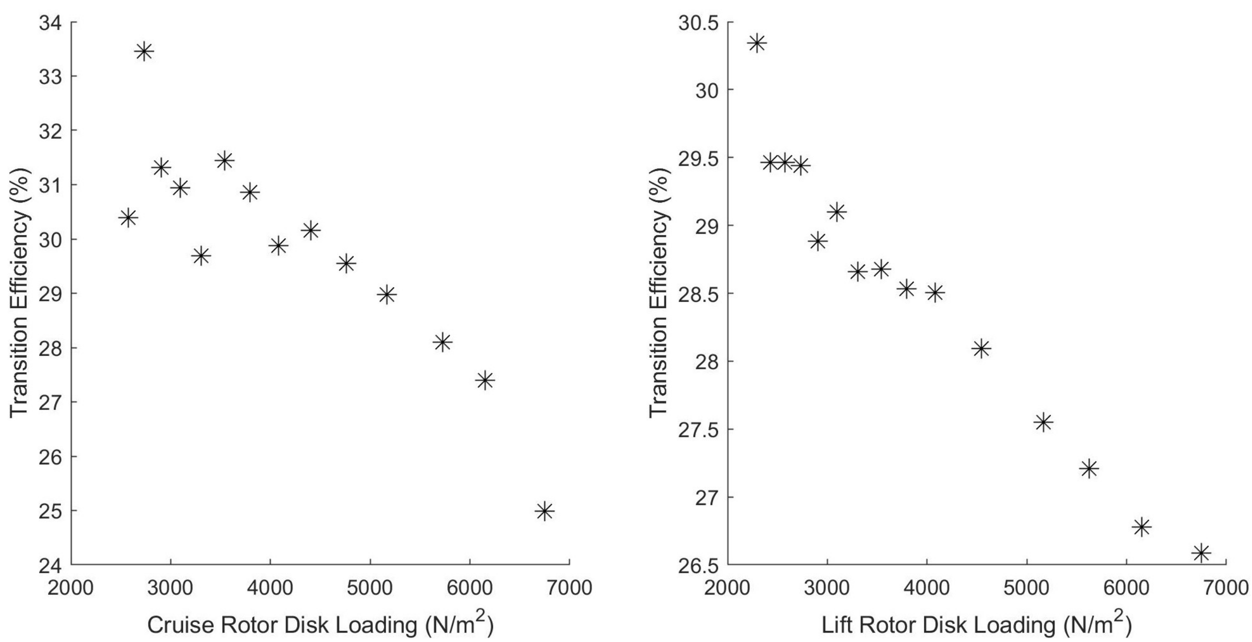

Fig. 6 Transition efficiency versus disk loading.

We find that a 10% increase in cruise rotor disk area translates to a 1% increase in transition efficiency. A similar 10% increase in lift rotor disk area translates to a 0.5% increase in transition efficiency. These results show that energy consumption can be reduced during transition for the lift-plus-cruise aircraft if disk loading is decreased.

Each data point in Fig. 6 represents a solution to the transition optimization problem. To generate this data the optimizer convergence tolerance was increased from 0.1 to 1. This increase in tolerance likely accounts for the variation in results towards the extremes of rotor disk loading.

V. Conclusion

In this paper, we present a methodology for optimizing the transition trajectory for the NASA lift-plus-cruise aircraft. We use direct transcription to formulate the optimal trajectory as a nonlinear programming problem that can be solved with gradient-based optimization. For this optimal trajectory we show time histories of design variables and aircraft states, and end by describing the effect of varying rotor disk loading on transition efficiency.

Little research exists on trajectory optimization for electric vertical takeoff and landing (eVTOL) aircraft. The prior work in the literature either uses low-order aerodynamic models, or focuses on tail-sitter UAVs, as opposed to the much larger eVTOL aircraft. This paper addresses this by finding optimal minimum-energy transition trajectories for NASA's lift-plus-cruise aircraft. The results presented here provide some insight into optimal eVTOL transition maneuvers.

We build a trajectory optimization algorithm that is constructed from a unique combination of models and methods. Notably we use nonlinear flight dynamics and model rotor aerodynamics using blade element momentum (BEM) theory. These models are implemented within a framework that uses adjoint derivatives. This methodology has the potential to scale well to trajectory optimization problems of even greater complexity.

The BEM rotor model used in this paper is a significant improvement over purely momentum-based models. However, it does not accurately consider edge-wise flight. Future work will incorporate a dynamic inflow model to address this limitation, as well as higher-fidelity lift and drag models for the lifting surfaces. Further work to assess aircraft stability and controllability along the optimal trajectory is also planned.

VI. Acknowledgments

The material presented in this paper is, in part, based upon work supported by NASA under award No. 80NSSC21M0070. The authors would like to thank Marius Ruh for his help in implementing the BEM rotor model and Mark Sperry for his help implementing the Ozone ODE solver.

References

[1] Ritz, R., and D'Andrea, R., "A global controller for flying wing tailsitter vehicles," *IEEE International Conference on Robotics and Automation (ICRA)*, 2017, pp. 2731–2738. https://doi.org/10.1109/ICRA.2017.7989318.

[2] Jung, Y., and Shim, D. H., "Development and Application of Controller for Transition Flight of Tail-Sitter UAV," *Journal on Intelligent Robotic Systems*, Vol. 65, 2012, p. 137–152. https://doi.org/10.1007/s10846-011-9585-1.

[3] Hartmann, P., Carsten, M., and Dieter, M., "Unified Velocity Control and Flight State Transition of Unmanned Tilt-Wing Aircraft," *Journal of guidance, control, and dynamics*, Vol. 40, No. 6, 2017, pp. 1348–1359. https://doi.org/10.2514/1.G002168.

[4] Cook, J., and Hauser, J., "Transition to Hover for a Flying Wing with Electric Propulsion," *Annual American Control Conference (ACC)*, 2018, pp. 2237–2242. https://doi.org/10.23919/ACC.2018.8431242.

[5] Raab, S. A., Zhang, J., Bhardwaj, P., and Holzapfel, F., "Proposal of a Unified Control Strategy for Vertical Take-off and Landing Transition Aircraft Configurations," *Applied Aerodynamics Conference*, 2018. https://doi.org/10.2514/6.2018-3478.

[6] Zhou, J., Lyu, X., Li, Z., Shen, S., and Zhang, F., "A unified control method for quadrotor tail-sitter UAVs in all flight modes: Hover, transition, and level flight," *IEEE/RSJ International Conference on Intelligent Robots and Systems (IROS)*, 2017, pp. 4835–4841. https://doi.org/10.1109/IROS.2017.8206359.

[7] Casau, P., Cabecinhas, D., and Silvestre, C., "Autonomous Transition Flight for a Vertical Take-Off and Landing aircraft," *50th IEEE Conference on Decision and Control and European Control Conference*, 2011, pp. 3974–3979. https://doi.org/10.1109/CDC.2011.6160819.

[8] Betts, J. T., "Survey of Numerical Methods for Trajectory Optimization," *Journal of Guidance, Control, and Dynamics*, Vol. 21, No. 2, 1998, pp. 193–207. https://doi.org/10.2514/2.4231.

[9] Chauhan, S. S., and Martins, J., "Tilt-Wing eVTOL Takeoff Trajectory Optimization," *Journal of Aircraft*, Vol. 57, No. 1, 2020, pp. 93–112. https://doi.org/10.2514/1.C035476.

[10] Anderson, R., Willis, J., Johnson, J., Ning, A., and Beard, R. W., "A Comparison of Aerodynamics Models for Optimizing the Takeoff and Transition of a Bi-Wing Tailsitter," *AIAA Scitech Forum*, 2021. https://doi.org/10.2514/6.2021-1008.

[11] Yang, Y., Yang, J., Wang, X., and Zhu, J., "Robust optimal transition maneuvers control for tail-sitter unmanned aerial vehicles," *International Journal on Robust Nonlinear Control*, Vol. 31, 2021, pp. 8007–8029. https://doi.org/10.1002/rnc.5736.

[12] Piprek, P., and Holzapfel, F., "Robust Trajectory Optimization of VTOL Transition Maneuver Using Bi-Level Optimal Control," *31st Congress of the International Council of the Aeronautical Sciences*, 2018, pp. 9–14.

[13] Stone, R. H., and Clarke, G., "Optimization of Transition Maneuvers for a Tail-Sitter Unmanned Air Vehicle," *Australian Aerospace International Congress*, 2001.

[14] Stone, R. H., Anderson, P., Hutchison, C., Tsai, A., Gibbens, P., and Wong, K. C., "Flight testing of the T-wing tail-sitter unmanned air vehicle," *Journal of Aircraft*, Vol. 45, No. 2, 2008, pp. 673–685. https://doi.org/10.2514/1.32750.

[15] Banazadeh, A., Assadian, N., and Saghafi, F., "Minimum time trajectory optimization of a tail-sitter aerial vehicle using nonlinear programming," *International Conference on Advanced Mechatronic Systems*, 2012, pp. 275–280.

[16] Banazadeh, Afshin, and Taymourtash, N., "Optimal Control of an Aerial Tail Sitter in Transition Flight Phases," *Journal of Aircraft*, Vol. 53, No. 4, 2016, p. 914–921. https://doi.org/10.2514/1.C033339.

[17] Kubo, D., and Suzuki, S., "Tail-Sitter Vertical Takeoff and Landing Unmanned Aerial Vehicle: Transitional Flight Analysis," *Journal of Aircraft*, Vol. 45, No. 1, 2008, pp. 292–297. https://doi.org/10.2514/1.30122.

[18] Zhong, J., and Wang, C., "Transition characteristics for a small tail-sitter unmanned aerial vehicle," *Chinese Journal of Aeronautics*, Vol. 34, No. 10, 2021, pp. 220–236. https://doi.org/10.1016/j.cja.2020.12.021.

[19] Li, B., Sun, J., Zhou, W., Wen, C. Y., Low, K. H., and Chen, C. K., "Transition Optimization for a VTOL Tail-Sitter UAV," *IEEE/ASME Transactions on Mechatronics*, Vol. 25, No. 5, 2020, pp. 2534–2545. https://doi.org/10.1109/TMECH.2020.2983255.

[20] Silva, C., Johnson, W. R., Solis, E., Patterson, M. D., and Antcliff, K. R., "VTOL Urban Air Mobility Concept Vehicles for Technology Development," *Aviation Technology, Integration, and Operations Conference*, 2018. https://doi.org/10.2514/6.2018-3847.

[21] Maqsood, A., and Go, T. H., "Optimization of Transition Maneuvers Through Aerodynamic Vectoring," *Aerospace Science and Technology*, Vol. 23, No. 1, 2012, pp. 363–371. https://doi.org/10.1016/j.ast.2011.09.004.

[22] Oosedo, A., Abiko, S., Konno, A., and Uchiyama, M., "Optimal Transition from Hovering to Level-Flight of a Quadrotor Tail-Sitter UAV," *Autonomous Robots*, Vol. 41, No. 5, 2017, pp. 1143–1159. https://doi.org/10.1007/s10514-016-9599-4.

[23] Verling, S., Stastny, T., Battig, G., Alexis, K., and Siegwart, R., "Model Based Transition Optimization for a VTOL Tailsitter," *IEEE International Conference on Robotics and Automation (ICRA)*, 2008, pp. 3939–3944. https://doi.org/10.1109/icra.2017.7989454.

[24] Pradeep, P., and Wei, P., "Energy Optimal Speed Profile for Arrival of Tandem Tilt-Wing eVTOL Aircraft with RTA Constraint," *IEEE CSAA Guidance, Navigation and Control Conference (CGNCC)*, 2018, pp. 1–6. https://doi.org/10.1109/GNCC42960.2018.9018748.

[25] Rothhaar, P. M., Murphy, P. C., Bacon, B. J., Gregory, I. M., Grauer, J. A., Busan, R. C., and Croom, M. A., "NASA Langley Distributed Propulsion VTOL TiltWing Aircraft Testing, Modeling, Simulation, Control, and Flight Test Development," *14th AIAA Aviation Technology, Integration, and Operations Conference*, 2014. https://doi.org/10.2514/6.2014-2999.

[26] Hwang, J. T., and Ning, A., "Large-Scale Multidisciplinary Optimization of an Electric Aircraft for On-Demand Mobility," *AIAA/ASCE/AHS/ASC Structures, Structural Dynamics, and Materials Conference*, 2018. https://doi.org/10.2514/6.2018-1384.

[27] Ruh, M. L., and Hwang, J. T., "Robust Modeling and Optimal Design of Rotors Using Blade Element Momentum Theory," *AIAA Aviation Forum*, 2021. https://doi.org/10.2514/6.2021-2598.

[28] Hwang, J. T., and Munster, D., "Solution of Ordinary Differential Equations in Gradient-Based Multidisciplinary Design Optimization," *AIAA/ASCE/AHS/ASC Structures, Structural Dynamics, and Materials Conference*, 2018. https://doi.org/10.2514/6.2018-1646.

[29] Martins, J., and Hwang, J. T., "Review and Unification of Methods for Computing Derivatives of Multidisciplinary Computational Models," *AIAA Journal*, Vol. 51, No. 11, 2013, pp. 2582–2599. https://doi.org/10.2514/1.J052184.

[30] Schmidt, D. K., *Modern Flight Dynamics*, Anderson Series, McGraw Hill, New York, 2012, pp. 445–478.

[31] Hwang, J. T., and Martins, J., "A fast-prediction surrogate model for large datasets," *Aerospace Science and Technology*, Vol. 75, 2018, pp. 74–87. https://doi.org/10.1016/j.ast.2017.12.030.

[32] Gill, P. E., Murray, W., and Saunders, M. A., "SNOPT: An SQP Algorithm for Large-Scale Constrained Optimization," *SIAM Review*, Vol. 47, No. 1, 2005, pp. 99–131. https://doi.org/10.1137/S0036144504446096.